Inorganic Chemistry
Cite This: Inorg. Chem. 2019, 58, 4110−4116
Article
pubs.acs.org/IC

Integrated Synthesis of Gold Nanoparticles Coated with Polyoxometalate Clusters

Sergio Martín,[†] Yohei Takashima,[†] Chang-Gen Lin,[‡] Yu-Fei Song,[‡] Haralampos N. Miras,*[,†] and Leroy Cronin*[,†]

[†]School of Chemistry, University of Glasgow, Glasgow G12 8QQ, U.K.

[‡]Beijing Advanced Innovation Center for Soft Matter Science and Engineering, State Key Laboratory of Chemical Resource Engineering, Beijing University of Chemical Technology, Beijing 100029, P. R. China

Supporting Information

ABSTRACT: Polyoxometalates (POMs) have been found to be good end-capping ligands for gold nanoparticles (AuNPs). Herein, we introduce a new synthetic method to synthesize gold nanoparticle−POM hybrids by heating a solution of $AuNO_3(PMe_3)$ in acetonitrile in the presence of appropriate POM species with tetrabutylammonium (TBA) as a countercation at 120 °C in a microwave. This method allowed us to produce POM-capped AuNPs without over-reduction of the solution causing decomposition or reorganization of the POMs. Analysis of the resulting material by transmission electron microscopy showed that the POM's size, charge, and functionality are key factors controlling the resulting POM−AuNP hybrid structure. Additionally, the reaction was monitored by electrospray ionization mass spectrometry (ESI-MS), ultraviolet−visible spectroscopy, and dynamic light scattering. The ESI-MS studies reveal crucial information regarding the nature of the reaction that takes place, showing the cation exchange between Au(I) and TBA cations, followed by self-reduction of the $Me_3PAu(I)$−POM complex.

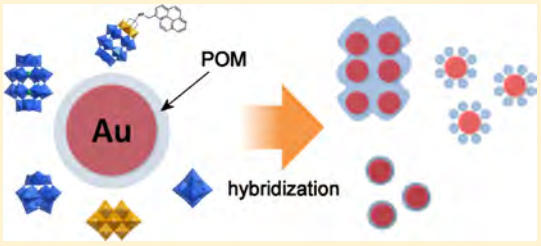

INTRODUCTION

Polyoxometalates (POMs) are discrete negatively charged inorganic metal oxide clusters with fascinating properties and applications in diverse research areas ranging from catalysis to medicine and biology.[1−7] This is because POM clusters represent a large family of compounds that exhibit a wide range of shapes, sizes, and topologies. Because of their polyanionic nature, structural diversity, and redox properties, POMs also have been employed as end-capping ligands for nanoparticle synthesis.[8,9] Exploration of their redox activity led to the development of various synthetic methodologies for nanoparticle formation: (1) chemical reduction (the use of chemical reductants such as $NaBH_4$, H_2, ascorbic acid, and Zn triggers the formation of POM nanoparticles),[10−15] (2) photochemical reduction [POMs can act as reducing agents as well as end-capping ligands upon photoreduction by ultraviolet (UV) light irradiation[16−20] or γ irradiation],[21] (3) electrochemical reduction (reduced POMs generated by bulk electrolysis and later used as reductants for the synthesis of nanoparticles),[22,23] and (4) reduction by POMs with "built-in reducing ability" [POMs with d-electron-containing metal ions (for example Mo^{V} or V^{IV}) have intrinsically reducing ability, enabling nanoparticle synthesis in the absence of chemical additives and/or external stimuli].[24−26]

Alternatively, POM-capped nanoparticles can also be synthesized following a ligand exchange approach. For example, alkanethiol or citrate ligands can be exchanged successfully with a POM species.[27,28] The main advantage of this method is the mild reaction conditions that are employed, without utilization of complex routes and over-reduction of the system that can be a problem for the stabilization of NPs by different POM structures. Weinstock and co-workers have achieved great success in developing rational synthetic approaches for coating the surfaces of nanoparticles with POM ligands followed by detailed characterization with cryo-transmission electron microscopy (cryo-TEM).[29−31] Their method is robust with careful control of the pH and redox potential.

Herein, we report a new synthetic method for forming gold nanoparticle−POM hybrids (AuNP−POMs) without involving reduction of the POM species. The hybrids were easily synthesized upon heating both the gold and POM precursors. In addition, the resulting hybrids exhibited different levels of nanoparticle surface coating depending on the size, charge, and functionality of the POMs (Figure 1). The reaction was also monitored using electrospray ionization mass spectrometry (ESI-MS), which has been proven to be a powerful tool for monitoring reactions and revealing details of reactivity and formation of intermediate species. Additionally, ESI-MS can be used to identify the nature of the intermediates and compositions of coordination, organometallic, and cluster compounds.[32−34] In this case, ESI-MS studies revealed some information regarding the first step of the reaction involving

Received: October 24, 2018
Published: March 14, 2019

DOI: 10.1021/acs.inorgchem.8b03013
Inorg. Chem. 2019, 58, 4110−4116

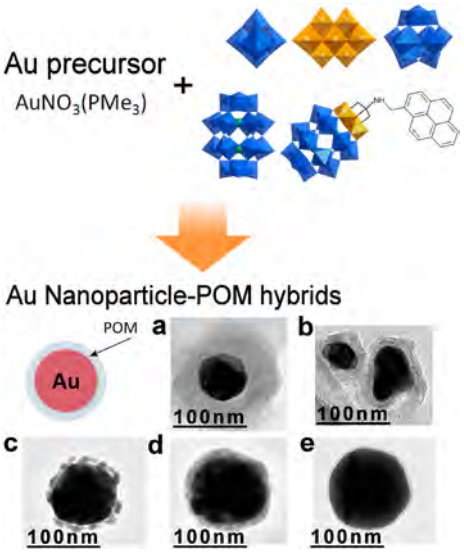

Figure 1. Schematic image of a gold nanoparticle–POM hybrid using (a) W_6, (b) V_{10}, (c) W_{12}, (d) W_{18}, and (e) $W_{15}V_3$-pyrene. The average diameter of the NP in the bottom three images is 100 nm.

the cation exchange between $AuNO_3(PMe_3)$ and POMs and the thermally induced reduction of Au(I)–POM complexes. Finally, dynamic light scattering (DLS) was used to monitor the growth of the gold nanoparticles.

RESULTS AND DISCUSSION

Synthesis of Gold Nanoparticle–POM Hybrids. We selected $AuNO_3(PMe_3)$ as a metal precursor for formation of the AuNP hybrids because there is precedent for describing the observation that it can decompose to metallic Au after undergoing a thermally induced reduction process.[35] Indeed, in our experiments, we found that a brown powder was obtained by heating $AuNO_3(PMe_3)$, which we determined to be metallic gold by powder X-ray diffraction (PXRD) measurements (Figure. 2a). The decomposition process in

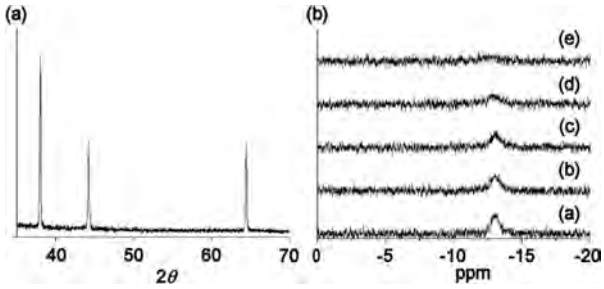

Figure 2. (a) PXRD patterns of gold metal synthesized by heating the CH_3CN solution with $AuNO_3(PMe_3)$ at 120 °C. The three peaks observed (2θ = 38.0°, 44.2°, and 64.6°) correspond to the diffractions from the {1 1 1}, {2 0 0}, and {2 2 0} planes of face-centered cubic gold, respectively. (b) ^{31}P NMR spectra of $AuNO_3(PMe_3)$ in CD_3CN after being heated at 85 °C for (a) 0, (b) 3 (c) 5, (d) 20, and (e) 90 h.

solution was also confirmed by ^{31}P nuclear magnetic resonance (NMR) (Figure 2b), showing the decrease in peak intensity associated with the precursor.

The gold nanoparticle–POM hybrids were successfully synthesized upon microwave heating of a CH_3CN solution of $AuNO_3(PMe_3)$ in the presence of appropriate POM species at 120 °C. Although it appears that a $AuNO_3(PMe_3)$ precursor is crucial, we did not attempt to elucidate the mechanism in this work, initially focusing on the phenomenological results demonstrating the integrated formation of AuNP–POM hybrids according to the following scheme:

$$Au(I)(NO_3)PMe_3 \xrightarrow[POM(TBA)_n]{\text{microwave}} Au(o)NPs$$

The effect on AuNP–POM hybrid formation utilizing six different POM species with different sizes, overall charges, and functionalities has been explored using the following clusters: $(TBA)_2[W_6O_{19}]$; $\{W_6\}$, $(TBA)_3[H_3V_{10}O_{28}]$; $\{V_{10}\}$, $(TBA)_4[H_4W_{12}O_{40}]$; $\{W_{12}\}$, $(TBA)_6[P_2W_{18}O_{62}]$; $\{W_{18}\}$, $(TBA)_5H[P_2W_{15}V_3O_{62}(NC_{21}H_{18})]$; $\{P_2W_{15}V_3\text{-pyrene}\}$ and $(TBA)_{13}H_{23}K_4[P_8W_{48}O_{184}]$; $\{W_{48}\}$ (TBA = tetrabutylammonium). It is worth noting that the POMs themselves do not appear to be reduced under the reaction conditions. Instead, the microwave heating induces the decomposition of the $Au(NO_3)PMe_3$, during which the color of the solution turns purple. However, the UV–visible (UV–vis) spectra of the solution after completion of the reaction exhibited clear differences depending on the POM species utilized (see Figure 3). The extent of surface coverage by POM species affects the

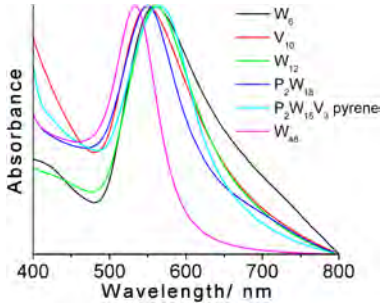

Figure 3. UV–vis spectra of gold nanoparticles with various POMs.

thickness of the POM layer as well as the average size distribution, which is reflected in the observed shifts in the UV–vis maxima.

In the case of $\{W_6\}$ and $\{V_{10}\}$, the gold nanoparticles were coated more effectively by POMs, even after the purification process, which results in the stabilization of nanoparticles. When using POMs with higher negative charges, better coverage of the NP's surface was achieved. In the case of $\{W_{12}\}$ with four negative charges, they were attached on the surface of the nanoparticle as small aggregates of approximately 5–7 nm. On the contrary, in the case of Dawson-type POMs $\{P_2W_{18}\}$ and $\{P_2W_{15}V_3\text{-pyrene}\}$, we observed a more homogeneous organization on the surface, with the $\{P_2W_{18}\}$ species exhibiting a slightly higher level of aggregation in comparison to that of the pyrene-derivatized species. Finally, the use of the largest available cluster, $\{W_{48}\}$, with the highest negative charge, led to the formation of highly aggregated NPs. In this case, electrostatic repulsions and steric hindrance prevented the POM clusters from effectively coating the NPs (see Figure 4).

The existence of POM-coated gold nanoparticles was confirmed by transmission electron microscopy (TEM), showing clear differences as a function of the POM's properties (Figure 5). Importantly, the reaction solutions were purified by dialysis treatment with a CH_3CN/H_2O mixed solvent, prior to the TEM measurements; during this process (Figure 5), POMs could show some level of organization on or around the gold

DOI: 10.1021/acs.inorgchem.8b03013
Inorg. Chem. 2019, 58, 4110–4116

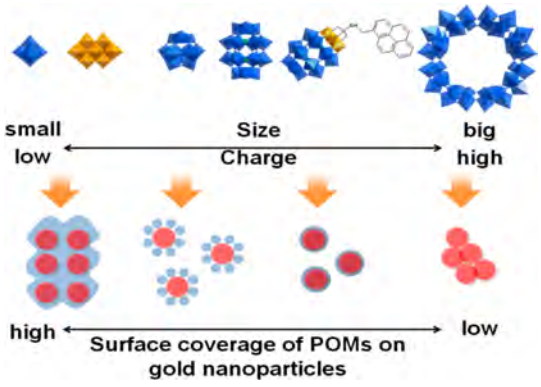

Figure 4. Conceptual representation of the observed surface coverage of nanoparticle–POM hybrids as a function of the POM's features.

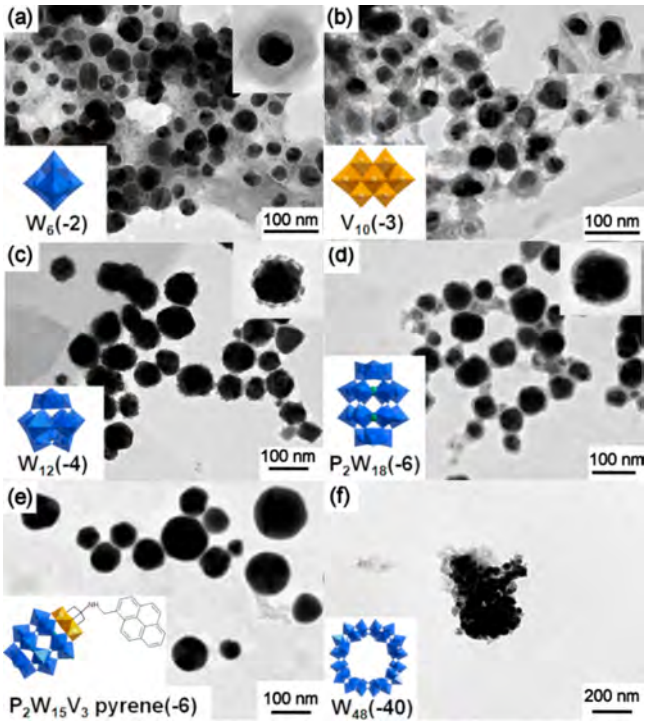

Figure 5. TEM images of gold nanoparticles with six kinds of POMs. Insets at the bottom left show POMs and their charges used in the syntheses. $\{W_6\}$, $(TBA)_2[W_6O_{19}]$; $\{V_{10}\}$, $(TBA)_3[H_3V_{10}O_{28}]$; $\{W_{12}\}$, $(TBA)_4[H_4W_{12}O_{40}]$; $\{P_2W_{18}\}$, $(TBA)_6[P_2W_{18}O_{62}]$; $\{P_2W_{15}V_3\text{pyrene}\}$, $(TBA)_5H[P_2W_{15}V_3O_{62}(NC_{21}H_{18})]$; $\{W_{48}\}$, $(TBA)_{13}H_{23}K_4[P_8W_{48}O_{184}]$. Insets at the top right show high-magnification images.

nanoparticles, accompanied by the removal of excess POMs. In addition, energy-filtered TEM (EFTEM) measurements were conducted to investigate the distribution of gold nanoparticles and POMs, showing that the gold nanoparticles were surrounded by POMs (Figure 6).

The differences observed in the hybrids formed depend greatly upon the size and charge of the POM species utilized (Figure 6). In the case of $\{W_6\}$ and $\{V_{10}\}$, which are small and have overall negative charges, they showed a tendency to aggregate more easily even in solution due to minimum steric and electrostatic repulsion. A lower coverage of $\{V_{10}\}$ compared to that of $\{W_6\}$ also supports this finding. This may be due to the fact that stronger repulsion leads to smaller POM aggregates, resulting in a small domain for $\{W_{12}\}$ and

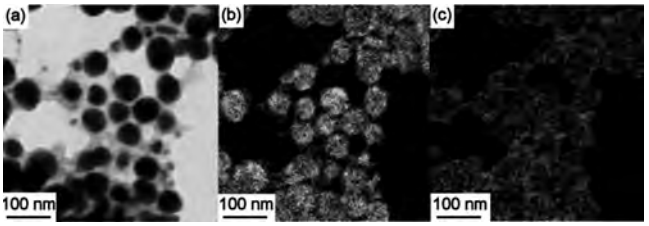

Figure 6. (a) Bright field TEM image of a gold nanoparticle with $\{P_2W_{18}\}$ and corresponding EFTEM images showing (b) Au and (c) W elements.

layer formation for $\{P_2W_{18}\}$ and $\{P_2W_{15}V_3\text{-pyrene}\}$. The lower POM coverage observed in the case of $\{P_2W_{15}V_3\text{-pyrene}\}$ is also likely due to steric hindrance induced by the pyrene group leading to less aggregation. In contrast, almost all of the $\{W_{48}\}$ species were removed during the purification process, presumably due to a high degree of electrostatic repulsion. Additionally, the wheel-shaped $\{W_{48}\}$ appears to interact less well with the surface of the nanoparticles.

TEM studies of the reaction mixtures showed the inability of $\{W_{48}\}$ species to interact efficiently with the gold nanoparticles. Instead, the AuNPs formed were spatially separated by the $\{W_{48}\}$ species, resulting in a narrower absorption band in the UV–vis spectrum (Figure 3). These results indicated that the aggregation of NPs depends upon the size and charge of the POMs and consequently their ability to allow effective surface coverage.

Monitoring the Reaction with UV–Vis and DLS. In an effort to investigate aspects of the reaction that leads to the formation for POM–NP complexes, we monitored the reaction by UV–vis and DLS measurements in the case of $\{W_{12}\}$. The UV–vis spectra showed a shift of the absorption band from 545 to 560 nm accompanied by an increase in the absorbance maximum (Figure 7a). Figure 7b shows the

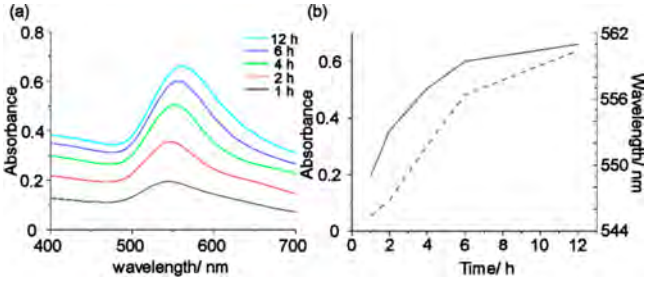

Figure 7. UV–vis data recorded during gold nanoparticle synthesis in the presence of $(TBA)_4[H_4W_{12}O_{40}]$. (a) Selected UV–vis spectra showing the evolution of the surface plasmon resonance peak. (b) Intensity absorbance maxima and observed shift of the plasmon resonance peak in the spectrum as a function of time.

position and intensity of the plasmon resonance band as a function of reaction time. The rapid increase in absorbance up to 6 h indicates fast formation of particles. As such, the DLS measurements allowed the collection of more direct information regarding the size and number of the nanoparticles. Figure 8 reveals an increase in particle size is accompanied by a small increase in the polydispersity of particles without a change in the average number.

Moreover, between 4 and 6 h, the particle size suddenly increases to 20 nm, which is accompanied by a decrease in their population that is in agreement with the coalescence of

DOI: 10.1021/acs.inorgchem.8b03013
Inorg. Chem. 2019, 58, 4110–4116

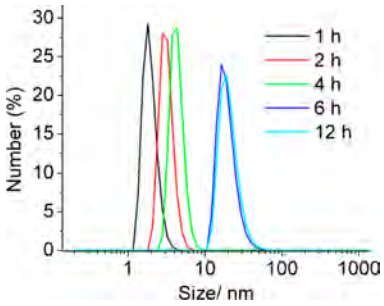

Figure 8. DLS data recorded during gold nanoparticle synthesis in the presence of $(TBA)_4[H_4W_{12}O_{40}]$ after heating for 1, 2, 4, 6, and 12 h.

the particles. The increase in particle concentration and the relatively weak coordination ability of POMs seem to be responsible for the coalescence. Finally, between 6 and 12 h, the experiments revealed very small changes in particle size, suggesting that most of the $Au(NO_3)PMe_3$ has already been consumed in the early stages of the reaction.

Monitoring the Reaction with ESI-MS. ESI-MS is a powerful tool for the precise determination of the composition and speciation of reaction mixtures.[36−40] To investigate the reaction that leads to the formation of NP−POM hybrids in more detail, ESI-MS measurements were conducted before and after the reaction. The spectrum obtained from the mixture before the reaction (Figure 9a) clearly shows peaks that can be assigned to $(TBA)NO_3$ and $Au(NO_3)PMe_3$, indicating that the TBA cations associated with the POM species can easily undergo a cation exchange process with the gold(I) cation even at ambient temperature. Additionally, it was possible to identify peaks associated with the complex formed between Au(I) and POM in the high-m/z region (Figure 9b). It is worth noting that no reaction occurs in the case in which $AuClPMe_3$ was used as a gold precursor. This initial cation exchange step is key for the effective stabilization of nanoparticles by the POMs that will form upon the reduction of the Au(I) source. The low-m/z region of the spectrum recorded from the reaction mixture upon completion of the reaction (Figure 9c) showed a decrease in the intensity of the peak associated with $Au(NO_3)PMe_3$, which indicates the consumption of the Au(I) source during nanoparticle formation and the appearance of a new small peak that could be assigned to $Au(NO_3)(PMe_3)_2$. The appearance of $Au(NO_3)(PMe_3)_2$ suggests that unreacted traces of $Au(NO_3)$-PMe_3 trap free PMe_3 groups produced from the decomposition of $Au(NO_3)PMe_3$. The high-m/z region of the spectrum provides additional evidence of the initial stages of the reaction (Figure 9d); most of the peaks initially associated with the complexes between $Au(NO_3)PMe_3$ and $\{W_{12}\}$ clusters appeared to have their intensity dramatically reduced after the reaction. On the other hand, the intensities of peaks assigned to the gold−POM complexes associated with one TBA (m/z 1655−1700) and without TBA (m/z 1529−1572) cations increased, while those of the species associated with two TBA cations (m/z 1800−1835) have been decreased, indicating that the cation exchange between TBA and the gold cation plays a key role during the reaction.

The combination of data obtained from UV−vis, DLS, and ESI-MS revealed some important information in regard to the species involved in the reaction that takes place in this case, and it is shown in Figure 10. The formation of nanoparticles

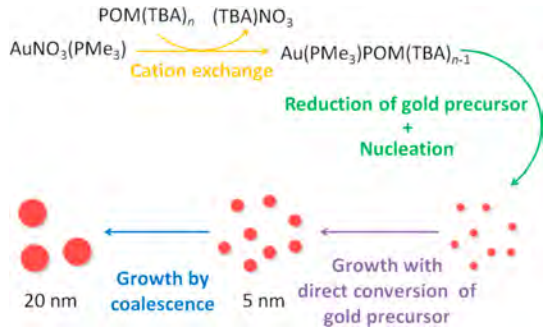

Figure 10. Schematic representation of the reaction steps leading to the formation of POM−NP hybrids.

observed at the early stages of the reaction is associated with the decomposition of gold−POM complexes triggered by a cation exchange process between the $Au(NO_3)PMe_3$ and $\{W_{12}\}$ species followed by a rapid increase in their average size. The observed increase in the size of the nanoparticles is based on the coalescence of the nanoparticles as a function of time

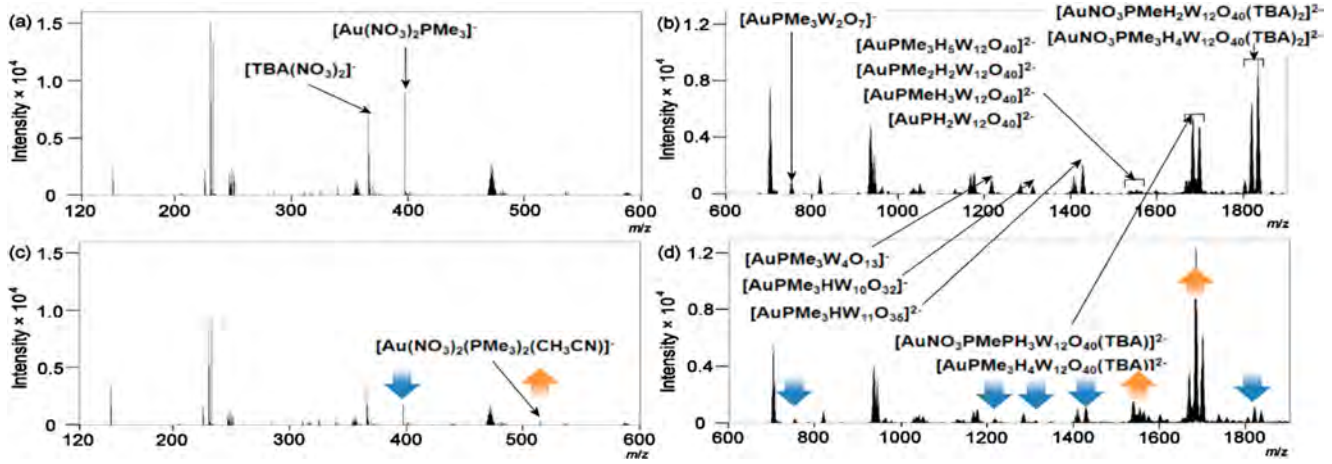

Figure 9. ESI-MS spectra of the $AuNO_3(PMe_3)/(TBA)_4[H_4W_{12}O_{40}]$ reaction mixture (a) before reaction (m/z 120−600), (b) before reaction (m/z 600−1900), (c) after reaction (m/z 120−600), and (d) after reaction (m/z 600−1900). Orange and blue arrows indicate increases and decreases in their peak intensities after reaction, respectively.

DOI: 10.1021/acs.inorgchem.8b03013
Inorg. Chem. 2019, 58, 4110−4116

(Figure S2†). It has been reported that the existence of the Au(III) intermediate species is due to disproportionation;[41−43] however, we were not able to detect any Au(III) species during the ESI-MS studies, suggesting that Au(I) is directly reduced to Au(0). This is potentially important in terms of the efficiency and prevention of potential side reactions that could affect the atom economy and/or the homogeneity of the hybrids generated.

CONCLUSIONS

In conclusion, we have introduced a new and easy synthetic method for preparing gold nanoparticle−POM hybrids. The presence of the POM species in solution is crucial for the prevention of uncontrolled and random aggregation of NPs. We have demonstrated that the POMs provide an elegant, energy efficient, and facile way to initiate the reduction and subsequent controlled growth of Au-NPs. We also showed that smaller POMs such as $\{W_6\}$ and $\{V_{10}\}$ with smaller negative charges could easily coat and stabilize NPs due to their weaker steric and electronic repulsions, leading to more efficient coating of the surface of gold nanoparticles with POM species. Additionally, larger POMs with a high negative charge demonstrated different interactions, which influences the surface's coating of gold nanoparticles. In the case of $\{W_{12}\}$ and $\{P_2W_{18}\}$, clusters form uniform POM layers on the surface, while in the case of $\{W_{48}\}$, no distinct surface organization was observed.

Finally, we also demonstrated that ESI-MS spectroscopy can be useful for monitoring the different species that form during the reaction of the starting materials and are crucial for the further development of NPs; the cation exchange between $AuNO_3(PMe_3)$ and POM species has been proven to be a crucial step at the early stages of the reaction and subsequent initiation of gold nanoparticle formation during heat-induced reduction. Moreover, UV−vis absorption and DLS were used to monitor the direct conversion of the gold precursor to gold nanoparticles followed by further rapid growth. Our observations are summarized in Figure 10.

A noteworthy advantage of this synthetic method is the fact that it is possible to form gold nanoparticle−POM hybrids without the use of additional internal (e.g., chemical reductants) or external (e.g., UV light irradiation) stimuli. This is important because it allows us to use any known POM species with various topologies and charges, including those that are unstable to chemical reduction or photoreduction. Because of the fascinating electrochemical properties of POMs, the new nanoparticle−POM hybrids would be expected to be promising candidates for the development of a new type of electronic and optoelectronic devices. For example, facile transport of charge carriers could occur compared to the case of the nanoparticles with organic capping ligands. Furthermore, nanoparticle−POM hybrids could also finely tune their surface plasmons via electrochemical reduction, which opens the door for the development of new sensors. Further studies of nanoparticle−POM hybrids along with detailed mechanistic investigations aiming to elucidate the products from the reduction process are underway.

EXPERIMENTAL SECTION

Synthesis. *$(TBA)_2[W_6O_{19}]$, $(TBA)_3[H_3V_{10}O_{28}]$, $(TBA)_4[H_4W_{12}O_{40}]$, $(TBA)_6[P_2W_{18}O_{62}]$, and $(TBA)_{13}H_{23}K_4[P_2W_{48}O_{184}]$.* The TBA salts of the POM clusters were synthesized according to previously reported methods.[44−46]

$(TBA)_5[HP_2W_{15}V_3O_{62}(C_{21}H_{19}N)]$. $(TBA)_5[H_4P_2V_3W_{15}O_{62}]$[47] (3.0 g, 0.58 mmol) is dissolved in 30 mL of acetonitrile. Tris-pyrene[48] $[(HOCH_2)_3CNH\text{-}CH_2\text{-}C_{16}H_9$, 200 mg, 0.60 mmol] is added, and the resulting solution is refluxed in the dark for 5 days. The solution is cooled to room temperature before being added dropwise to a large excess of diethyl ether with vigorous stirring to form a yellow precipitate. The precipitate is collected and redissolved in acetonitrile. Pure $(TBA)_5[HP_2W_{15}V_3O_{62}(C_{21}H_{19}N)]$ is obtained by re-precipitation in diethyl ether: yield 2.818 g, 0.52 mmol, 89%; ^{1}H NMR (400 MHz, CD_3CN) δ 9.20−7.10 (m, 8H), 5.93 (s, 2H), 5.64 (s, 6H) in addition to the TBA resonances. Anal. Calcd for $C_{101}H_{200}N_6P_2W_{15}V_3O_{62}$ (5463.04 g mol^{-1}): C, 22.21; H, 3.69; N, 1.54. Found: C, 22.24; H, 3.89; N, 1.68.

$AuNO_3(PMe_3)$. $AuNO_3(PMe_3)$ was synthesized according to a previous report.

Gold Nanoparticle−POM Hybrids. In a typical experiment, $AuNO_3(PMe_3)$ (7.7 mg, 25 μmol) and $(TBA)_4[H_4W_{12}O_{40}]$ (9.6 mg, 2.5 μmol) were dissolved in CH_3CN (20 mL) in a Pyrex microwave vial, and the sealed reaction mixture was then placed in a microwave reactor and heated to 120 °C for 12 h. The resulting purple solution with gold nanoparticles gives a crude yield of >50% in all cases. However, the crude material is contaminated with excess unreacted POMs. To purify the AuNP−POM hybrids, they were transferred into a dialysis membrane tube composed of cellulose (molecular weight cutoff of 3500) and dialyzed for 24 h using 1000 mL of the mixture containing CH_3CN and water [1:1 (v/v)] to remove unreacted $(TBA)_4[H_4W_{12}O_{40}]$, and this process was repeated twice. The use of a dialysis membrane was essential to remove any aggregates of unreacted POM species that prevented the observation of the POM−NP hybrids as evidenced by TEM of the reaction mixture before the dialysis process. The yield after dialysis in all cases was in the range of 4−5%. After the dialysis treatment, the solution was concentrated ∼10-fold by evaporation of the relevant amount of solvent, followed by deposition of the solution dropwise onto a carbon-coated TEM grid. The size distribution of gold nanoparticles was measured using calibrated TEM images by ImageJ (a public domain image and analysis processing program).

Characterization. UV−vis spectra were recorded using a JASCO V-670 spectrometer in absorbance mode using quartz cuvettes with a 1.0 cm optical path length. Microwave-assisted reactions were performed using a CEM Discovery microwave. DLS measurements were recorded using a Malvern Instruments Zetasizer Nano ZS instrument at 25 °C. ^{31}P NMR spectra were recorded on a Bruker DPX 400 instrument . All δ values are given in parts per million. PXRD patterns were recorded on a Philips X-pert diffractometer [λ(CuKα) = 1.5405 Å] equipped with a PW3710 control unit. ESI-MS measurements were taken at 30 °C using a Bruker micro ToF-Q instrument in negative ion mode. TEM and EFTEM images were recorded on a FEI Tecnai T20 transmission electron microscope equipped with a Gatan imaging filter.

ASSOCIATED CONTENT

Supporting Information

The Supporting Information is available free of charge on the ACS Publications website at DOI: 10.1021/acs.inorgchem.8b03013.

DLS, ESI-MS spectra, TEM images, and thermogravimetric analysis (PDF)

AUTHOR INFORMATION

Corresponding Authors

*E-mail: Charalampos.moiras@Glasgow.ac.uk.
*E-mail: lee.cronin@glasgow.ac.uk.

ORCID

Haralampos N. Miras: 0000-0002-0086-5173
Leroy Cronin: 0000-0001-8035-5757

DOI: 10.1021/acs.inorgchem.8b03013
Inorg. Chem. 2019, 58, 4110−4116

Notes

The authors declare no competing financial interest.

■ ACKNOWLEDGMENTS

The authors gratefully acknowledge financial support from the EPSRC for funding (Grants EP/L023652/1, EP/R020914/1, EP/L023652/1, EP/R01308X/1, EP/K023004/1, EP/H024107/1, EP/I033459/1, and EP/J015156/1) at the University of Glasgow and the ERC (Project 670467 SMART-POM), and L.C. thanks the Royal-Society Wolfson Foundation for a Merit Award. Y.-F.S. thanks the National Key Research and Development Program of China (2017YFB0307303), the National Nature Science Foundation of China (NFSC), and the Beijing Advanced Innovation Center for Soft Matter Science and Engineering (BAIC-SM) for financial support. The authors thank Donald A. MacLaren for EM measurements.

■ REFERENCES

(1) Pope, M. T.; Müller, A. Polyoxometalate Chemistry. *Angew. Chem., Int. Ed. Engl.* **1991**, *30*, 34−48.
(2) Miras, H. N.; Yan, J.; Long, D.-L.; Cronin, L. Engineering Polyoxometalates with Emergent Properties. *Chem. Soc. Rev.* **2012**, *41*, 7403−7430.
(3) Miras, H. N.; Vilà-Nadal, L.; Cronin, L. Polyoxometalate Based Open-Frameworks (POM-OFs). *Chem. Soc. Rev.* **2014**, *43*, 5679−5699.
(4) Mizuno, N.; Misono, M. Heterogeneous Catalysis. *Chem. Rev.* **1998**, *98*, 199−218.
(5) Kozhevnikov, I. V. Catalysis by Heteropoly Acids and Multicomponent Polyoxometalates in Liquid-Phase Reactions. *Chem. Rev.* **1998**, *98*, 171−198.
(6) Rhule, J. T.; Hill, C. L.; Judd, D. A.; Schinazi, R. F. Polyoxometalates in Medicine. *Chem. Rev.* **1998**, *98*, 327−358.
(7) Yamase, T. Photo- and Electrochromism of Polyoxometalates and Related Materials. *Chem. Rev.* **1998**, *98*, 307−326.
(8) (a) Keita, B.; Liu, T.; Nadjo, L. Synthesis of Remarkably Stabilized Metal Nanostructures Using Polyoxometalates. *J. Mater. Chem.* **2009**, *19*, 19−33. (b) Zhang, M.; Hao, J.; Neyman, A.; Wang, Y.; Weinstock, I. A. Influence of Polyoxometalate Protecting Ligands on Catalytic Aerobic Oxidation at the Surfaces of Gold Nanoparticles in Water. *Inorg. Chem.* **2017**, *56*, 2400−2408.
(9) Wang, Y.; Weinstock, I. A. Polyoxometalate-Decorated Nanoparticles. *Chem. Soc. Rev.* **2012**, *41*, 7479.
(10) (a) Zoladek, S.; Rutkowska, I. A.; Skorupska, K.; Palys, B.; Kulesza, P. J. Fabrication of Polyoxometallate-Modified Gold Nanoparticles and Their Utilization as Supports for Dispersed Platinum in Electrocatalysis. *Electrochim. Acta* **2011**, *56*, 10744−10750. (b) Ozkar, S.; Finke, R. G. Nanoparticle Nucleation is Tetramolecular in Metal and Involves Hydrogen: Evidence for a Kinetically Effective Nucleus of Three $\{Ir_3H_{2x}P_2W_{15}Nb_3O_{62}\}^{6-}$ in $Ir(0)_n$ Nanoparticle Formation From $[(1,5\text{-COD})Ir^{I}P_2W_{15}Nb_3O_{62}]^{8-}$ Plus Dihydrogen. *J. Am. Chem. Soc.* **2017**, *139*, 5444−5457.
(11) (a) Lin, Y.; Finke, R. G. Novel Polyoxoanion- and Bu4N+-Stabilized, Isolable, and Redissolvable, 20−30-.ANG. Ir300−900 Nanoclusters: The Kinetically Controlled Synthesis, Characterization and Mechanism of Formation of Organic Solvent-Soluble, Reproducible Size and Reproducible Catalytic Activity Metal Nanoclusters. *J. Am. Chem. Soc.* **1994**, *116*, 8335−8353. (b) Lin, Y.; Finke, R. G. A More General Approach to Distingushing "Homogeneous" from "Heterogeneous" Catalysis: Discovery of Polyoxoanion- and BuN_4^+ Stabilized, Isolable and Redissolvable, High-Reactivity Ir.apprx. 190−450 Nanocluster Catalysts. *Inorg. Chem.* **1994**, *33*, 4891−4910.
(12) Aiken, J. D.; Finke, R. G. Nanocluster Formation Synthetic, Kinetic, and Mechanistic Studies. The Detection of, and the Methods to Avoid, Hydrogen Mass-Transfer Limitations in the Synthesis of Polyoxoanion- and Tetrabutylammonium-Stabilized, Near- Monodisperse 40 ± 6 Å Rh(0) Nanoclusters. *J. Am. Chem. Soc.* **1998**, *120*, 9545−9554.
(13) Yuan, J. H.; Chen, Y. X.; Han, D. X.; Zhang, Y. J.; Shen, Y. F.; Wang, Z. J.; Niu, L. Synthesis of Highly Faceted Multiply Twinned Gold Nanocrystals Stabilized by Polyoxometalates. *Nanotechnology* **2006**, *17*, 4689−4694.
(14) Maayan, G.; Neumann, R. Direct Aerobic Epoxidation of Alkenes Catalyzed by Metal Nanoparticles Stabilized by the $H_5PV_2Mo_{10}O_{40}$ Polyoxometalate. *Chem. Commun.* **2005**, *36*, 4595.
(15) Maayan, G.; Neumann, R. Direct Aerobic Oxidation of Secondary Alcohols Catalysed by Pt(0) Nanoparticles Stabilized by $[PV_2Mo_{10}O_{40}]^{5-}$ Polyoxmetalate. *Catal. Lett.* **2008**, *123*, 41−45.
(16) Chalkley, L. The Extent of the Photochemical Reduction of Phosphotungstic Acid. *J. Phys. Chem.* **1952**, *56*, 1084−1086.
(17) Troupis, A.; Hiskia, A.; Papaconstantinou, E. Synthesis of Metal Nanoparticles by Using Polyoxometalates as Photocatalysts and Stabilizers. *Angew. Chem., Int. Ed.* **2002**, *41*, 1911−1914.
(18) Troupis, A.; Gkika, E.; Hiskia, A.; Papaconstantinou, E. Photocatalytic Reduction of Metals Using Polyoxometallates: Recovery of Metals or Synthesis of Metal Nanoparticles. *C. R. Chim.* **2006**, *9*, 851−857.
(19) Mandal, S.; Selvakannan, P. R.; Pasricha, R.; Sastry, M. Keggin Ions as UV-Switchable Reducing Agents in the Synthesis of Au Core-Ag Shell Nanoparticles. *J. Am. Chem. Soc.* **2003**, *125*, 8440−8441.
(20) Mandal, S.; Das, A.; Srivastava, R.; Sastry, M. Keggin Ion Mediated Synthesis of Hydrophobized Pd Nanoparticles for Multifunctional Catalysis. *Langmuir* **2005**, *21*, 2408−2413.
(21) Gordeev, A. V.; Kartashev, N. I.; Ershov, B. G. Metal Nanoparticles with $[PW_{11}O_{39}]^{7-}$ and $[P_2W_{17}O_{61}]^{10-}$ Heteropoly Anions as Stabilizing Agents: Radiation-Chemical Preparation and Properties. *High Energy Chem.* **2002**, *36*, 75−79.
(22) Zhang, G.; Keita, B.; Biboum, R. N.; Miserque, F.; Berthet, P.; Dolbecq, A.; Mialane, P.; Catala, L.; Nadjo, L. Synthesis of Various Crystalline Gold Nanostructures in Water: The Polyoxometalate β-$[H_4PMo_{12}O_{40}]^{3-}$ as the Reducing and Stabilizing Agent. *J. Mater. Chem.* **2009**, *19*, 8639.
(23) Hsu-Yao, T.; Browne, K. P.; Honesty, N.; Tong, Y. J. Polyoxometalate-stabilized Pt Nanoparticles and their Electrocatalytic Activities. *Phys. Chem. Chem. Phys.* **2011**, *13*, 7433.
(24) Zhang, G.; Keita, B.; Dolbecq, A.; Mialane, P.; Sécheresse, F.; Miserque, F.; Nadjo, L. Green Chemistry-Type One-Step Synthesis of Silver Nanostructures Based on Mo. *Chem. Mater.* **2007**, *19*, 5821−5823.
(25) Keita, B.; Zhang, G.; Dolbecq, A.; Mialane, P.; Sécheresse, F.; Miserque, F.; Nadjo, L. -Mo VI Mixed Valence Polyoxometalates for Facile Synthesis of Stabilized Metal Nanoparticles: Electrocatalytic Oxidation of Alcohols. *J. Phys. Chem. C* **2007**, *111*, 8145−8148.
(26) Liu, R.; Li, S.; Yu, X.; Zhang, G.; Zhang, S.; Yao, J.; Keita, B.; Nadjo, L.; Zhi, L. Facile Synthesis of Au-Nanoparticle/Polyoxometalate/Graphene Tricomponent Nanohybrids: An Enzyme-Free Electrochemical Biosensor for Hydrogen Peroxide. *Small* **2012**, *8*, 1398−1406.
(27) Lica, G. C.; Browne, K. P.; Tong, Y. J. Interactions Between Keggin-Type Lacunary Polyoxometalates and Ag Nanoparticles: A Surface-Enhanced Raman Scattering Spectroscopic Investigation. *J. Cluster Sci.* **2006**, *17*, 349−359.
(28) Ernst, A. Z.; Sun, L.; Wiaderek, K.; Kolary, A.; Zoladek, S.; Kulesza, P. J.; Cox, J. A. Synthesis of Polyoxometalate-Protected Gold Nanoparticles by a Ligand-Exchange Method: Application to the Electrocatalytic Reduction of Bromate. *Electroanalysis* **2007**, *19*, 2103−2109.
(29) Neyman, A.; Meshi, L.; Zeiri, L.; Weinstock, I. A. Direct Imaging of the Ligand Monolayer on an Anion-Protected Metal Nanoparticle Through Cryogenic Trapping of its Solution-State Structure. *J. Am. Chem. Soc.* **2008**, *130*, 16480−16481.
(30) Wang, Y.; Neyman, A.; Arkhangelsky, E.; Gitis, V.; Meshi, L.; Weinstock, I. A. Self-Assembly and Structure of Directly Imaged Inorganic-Anion Monolayers on a Gold Nanoparticle. *J. Am. Chem. Soc.* **2009**, *131*, 17412−17422.

DOI: 10.1021/acs.inorgchem.8b03013
Inorg. Chem. 2019, 58, 4110−4116

(31) Wang, Y.; Zeiri, O.; Sharet, S.; Weinstock, I. A. Role of the Alkali-Metal Cation Size in the Self-Assembly of Polyoxometalate-Monolayer Shells on Gold Nanoparticles. *Inorg. Chem.* **2012**, *51*, 7436−7438.
(32) Colton, R.; D'Agostino, A.; Traeger, J. C. Electrospray Mass Spectrometry Applied to Inorganic and Organometallic Chemistry. *Mass Spectrom. Rev.* **1995**, *14*, 79−106.
(33) Henderson, W.; Nickleson, B. K.; McCaffrey, L. J. Applications of Electrospray Mass Spectrometry in Organometallic Chemistry. *Polyhedron* **1998**, *17*, 4291−4313.
(34) Johnson, B. F. G., Jr.; McIndoe, J. S. Spectroscopic and Mass Spectrometric Method for the Characterisation of Metal Clusters. *Coord. Chem. Rev.* **2000**, *200−202*, 901−932.
(35) Yuan, Y.; Kozlova, A. P.; Asakura, K.; Wan, H.; Tsai, K.; Iwasawa, Y. Supported Au Catalysts Prepared from Au Phosphine Complexes and As-Precipitated Metal Hydroxides: Characterization and Low-Temperature CO Oxidation. *J. Catal.* **1997**, *170*, 191−199.
(36) Miras, H. N.; Wilson, E. F.; Cronin, L. Unravelling the Complexities of Inorganic and Supramolecular Self-Assembly in Solution with Electrospray and Cryospray Mass Spectrometry. *Chem. Commun.* **2009**, *0*, 1297−1311.
(37) Miras, H. N.; Long, D.-L.; Kögerler, P.; Cronin, L. Bridging the Gap Between Solution and Solid State Studies in Polyoxometalate Chemistry: Discovery of a Family of $[VM_{17}]$-Based Cages Encapsulating Two $\{V^{V}O4\}$ Moieties. *Dalton Trans.* **2008**, 214−221.
(38) Wilson, E. F.; Miras, H. N.; Rosnes, M. H.; Cronin, L. Real-Time Observation of the Self-Assembly of Hybrid Polyoxometalates Using Mass Spectrometry. *Angew. Chem., Int. Ed.* **2011**, *50*, 3720−3724.
(39) Yan, J.; Long, D.-L.; Miras, H. N.; Cronin, L. Cation Controlled Assembly and Transformation of Mono and Bi-Sulfite Templated Dawson-Type Polyoxotungstates. *Inorg. Chem.* **2010**, *49*, 1819−1825.
(40) Xu, F.; Scullion, R. A.; Yan, J.; Miras, H. N.; Busche, C.; Scandurra, A.; Pignataro, B.; Long, D. L.; Cronin, L. A Supramolecular Heteropolyoxopalladate $\{Pd_{15}\}$ Cluster Host Encapsulating a $\{Pd_2\}$ Dinuclear Guest: $[Pd^{II}{}_2\{H_7Pd^{II}{}_{15}O_{10}\ (PO_4)_{10}\}]^{9-}$. *J. Am. Chem. Soc.* **2011**, *133*, 4684−4686.
(41) Eustis, S.; El-Sayed, M. A. Molecular Mechanism of the Photochemical Generation of Gold Nanoparticles in Ethylene Glycol: Support for the Disproportionation Mechanism. *J. Phys. Chem. B* **2006**, *110*, 14014−14019.
(42) Bergamini, G.; Ceroni, P.; Balzani, V.; Gingras, M.; Raimundo, J.-M.; Morandi, V.; Merli, P. G. Synthesis of Small Gold Nanoparticles: Au(I) Disproportionation Catalyzed by a Persulfurated Coronene Dendrimer. *Chem. Commun. (Cambridge, U. K.)* **2007**, *1*, 4167−4169.
(43) Das, A. K.; Raj, C. R. Iodide-Mediated Reduction of $AuCl_4^-$ and a New Green Route for the Synthesis of Single Crystalline Au Nanostructures with Pronounced Electrocatalytic Activity. *J. Phys. Chem. C* **2011**, *115*, 21041−21046.
(44) Himeno, S.; Yoshihara, M.; Maekawa, M. Formation of Voltammetrically-Active Isopolyoxotungstate Complexes in Aqueous CH_3CN Media. *Inorg. Chim. Acta* **2000**, *298*, 165−171.
(45) McGlone, T.; Thiel, J.; Streb, C.; Long, D.-L.; Cronin, L. An Unprecedented Silver-Decavanadate Dimer Investigated Using Ion-Mobility Mass Spectrometry. *Chem. Commun.* **2012**, *48*, 359−361.
(46) Gabb, D.; Pradeep, C. P.; Boyd, T.; Mitchell, S. G.; Miras, H. N.; Long, D. L.; Cronin, L. A General Route for the Transfer of Large, Highly-Charged Polyoxometalates from Aqueous to Organic Phase. *Polyhedron* **2013**, *52*, 159−164.
(47) Finke, R. G.; Rapko, B.; Saxton, R. J.; Domaille, P. J. Trisubstituted Heteropolytungstates as Soluble Metal Oxide Analogs. III. Synthesis, Characterization, Phosphorus-31, Silicon-29, Vanadium-51, and 1- and 2-D Tungsten-183 NMR, Deprotonation, and Proton Mobility Studies of Organic Solvent Solute Forms of $[H_xSiW_9V_3O_{40}]^{x-7}$ and $[H_xP_2W_{15}V_3O_{62}]^{x-9}$. *J. Am. Chem. Soc.* **1986**, *108*, 2947−2960.
(48) Song, Y. F.; Long, D. L.; Cronin, L. Noncovalently Connected Frameworks with Nanoscale Channels Assembled from a Tethered Polyoxometalate-Pyrene Hybrid. *Angew. Chem., Int. Ed.* **2007**, *46*, 3900−3904.

DOI: 10.1021/acs.inorgchem.8b03013
Inorg. Chem. 2019, 58, 4110−4116